ELSEVIER

Journal of Alloys and Compounds 317–318 (2001) 443–447

Journal of ALLOYS AND COMPOUNDS

www.elsevier.com/locate/jallcom

# $R_9Mg_{34}Zn_{57}$ icosahedral quasicrystals: The tuning of a model spin glass

P.C. Canfield*, I.R. Fisher

*Ames Laboratory and Department of Physics and Astronomy, Iowa State University, Ames, IA 50011, USA*

**Abstract**

The growth of large single grains of face-centered icosahedral $R_9Mg_{34}Zn_{57}$ (R=Y, Gd–Er) quasicrystals (referred to as RMgZn from here on) has allowed the detailed study of the intrinsic properties of single phase samples that contain a quasiperiodic rare earth sublattice. By comparison of GdMgZn (Heisenberg moment) to TbMgZn or DyMgZn (non-Heisenberg moments) a clearly reduced freezing temperature ($T_f$) for GdMgZn can be observed. In order to explore this further pseudo-ternary series such as $(Y_{1-x}Gd_x)$MgZn, $(Tb_{1-x}Gd_x)$MgZn, $(Dy_{1-x}Gd_x)$MgZn, and $(Dy_{1-x}Tb_x)$MgZn were grown. Whereas $T_f$ changes monotonically with $x$ for the Gd/Y and Tb/Dy series, there is a rapid rise in $T_f$ for the addition of small amounts of the non-Heisenberg moments Tb or Dy into GdMgZn. For approximately 30% non-Heisenberg substitution on the Gd site $T_f$ passes through a local maximum and is reduced in a roughly linear manner for further increases in the concentration of non-Heisenberg moments. Analysis of these data lead to the conclusion that there is a threshold concentration of non-Heisenberg moments needed to force the whole system to act in a non-Heisenberg manner. 

*Keywords:* Spin glass; Quasicrystal; Freezing temperature; Magnetization; Single crystal

## 1. Introduction

In this paper we will try to make a few rather simple points: (i) The face-centered icosahedral $R_9Mg_{34}Zn_{57}$ (R=Y, Gd–Er) series (referred to as RMgZn from now on) is an ideal ground for testing ideas about spin glass physics, and (ii) there is a clear, experimentally measurable, difference between Heisenberg and non-Heisenberg spin glasses in the quasicrystalline RMgZn system and an apparent cross over from one type of behavior to the other with doping.

## 2. Sample growth and measurement

Single grains of RMgZn quasicrystals can be readily grown out of high temperature solution, in this case a self-flux of excess Mg and Zn [1]. This can be seen in Fig. 1 in which a pseudo-binary cut of the Y–Mg–Zn phase diagram is shown [1,2]. Although the icosahedral phase is incongruently melting, there is a well defined, and clearly exposed liquid–solidus surface for primary formation of the icosahedral YMgZn phase. YMgZn, as well as the other RMgZn members, is then an ideal candidate for solution growth [1,3,4]. The vertical arrow shown in Fig. 1 represents the initial composition of our melt as well as the initial cooling through the liquidus. The melt is further cooled to allow the growth of the single grains. A usual growth entails cooling from 650 to 450°C over 150 h (see Refs. [1,4,5] for details). At the end of the slow cooling, the remaining liquid is decanted from the single grains. The specific composition of the initial melt varies with R. Although initially [1,5] we were not able to grow pure GdMgZn, recently we have located enough of the liquid–solidus surface to allow for growth of single grains. For these growths an initial composition of $Gd_{26}Mg_{65}Zn_{32.4}$ was used.

The inset to Fig. 1 is a picture of a HoMgZn single quasicrystalline grain grown in this manner. As can be seen, the self-flux grown single grain manifests the morphology of a pentagonal dodecahedron. Single grains of RMgZn with linear dimensions as large as a centimeter have been grown using this technique. In addition, this technique has been extended to grow even larger grains of other quasicrystalline and related materials such as

*Corresponding author. Tel.: +1-515-294-6270; fax: +1-515-294-0689.

*E-mail address:* canfield@ameslab.gov (P.C. Canfield).

0925-8388/01/$ – see front matter 
PII: S0925-8388(00)01366-9

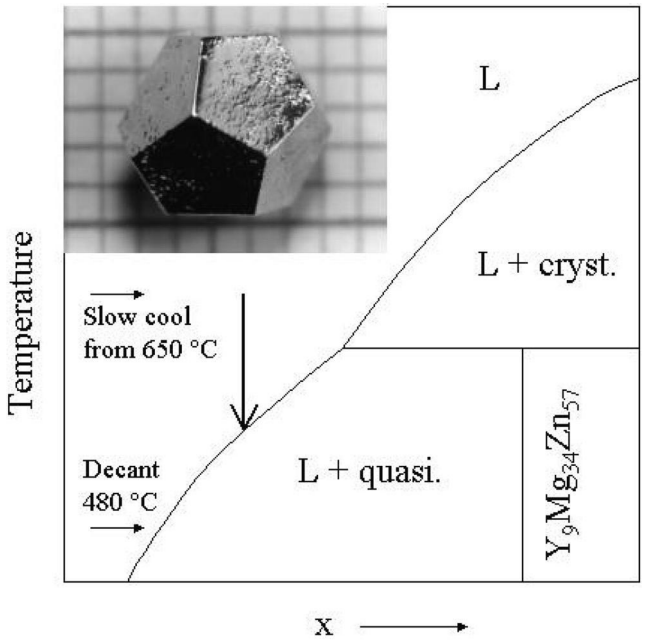


Fig. 1. (a) Schematic pseudo-binary cut of the Y–Mg–Zn phase diagram approximately along the $Y_xMg_{60-3x}Zn_{40-2x}$ line (based on Ref. [2]). Vertical arrow represents initial melt with composition $Y_3Mg_{51}Zn_{46}$. Note: neither axis is to scale. Inset: photograph of HoMgZn single grain over mm scale.

icosahedral AlMnPd [6], decagonal AlNiCo [7] and the $\xi'$ approximant of AlMnPd [4].

All the magnetic measurements have been taken on Quantum Design, SQUID magnetometers [5].

## 3. The spin glass state for Heisenberg and non-Heisenberg RMgZn

The magnetization ($M$) divided by the applied field ($H=25$ Oe) is plotted as a function of temperature for DyMgZn, TbMgZn and GdMgZn in Fig. 2. There are several points worth noting. First, for each compound there is a clear spin glass transition at $T_f$, below which there is a distinct irreversibility in the magnetization. This is examined in detail in Fig. 2b where for TbMgZn there are four curves between the zero-field-cooled (zfc) and field cooled (fc) curves. These are associated with starting from a zfc state at $T=1.8$ K and then warming to $T<T_f$, fc back down to 1.8 K and warming again. Irreversibility in such small applied fields below a critical temperature is characteristic behavior for a spin glass. As shown by Fisher et al. [5] the time and frequency dependent properties of RMgZn compounds are also characteristic of a model spin glass system. It appears that the aperiodicity of the R sites in this highly ordered icosahedral structure provides a reproducible method of creating a low temperature, spin glass ground state.

The second point of note in Fig. 2 is that whereas the

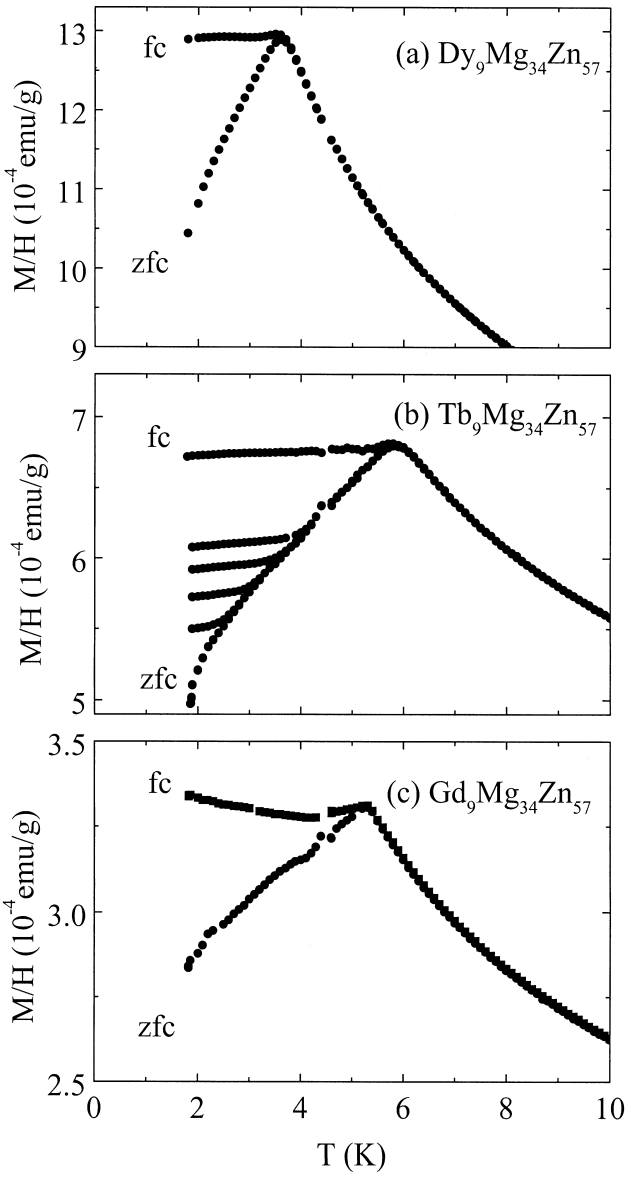


Fig. 2. Low field $M(T)/H$ for field cooled and zero field cooled runs with $H=25$ Oe: (a) DyMgZn, (b) TbMgZn, (c)GdMgZn.

freezing temperature of TbMgZn ($T_f=5.80$ K) is higher than that of DyMgZn ($T_f=3.60$ K), the freezing temperature of GdMgZn ($T_f=5.20$ K) is lower than that of TbMgZn. At first glance this is rather unusual, given that the de Gennes factor, $dG=(g_J-1)^2J(J+1)$ is larger for Gd than it is for Tb. To examine this in more detail the paramagnetic $\theta$, taken from the high temperature fit of the magnetic susceptibility to the Curie–Weiss Law $C=C/T-\theta$, as well as the freezing temperature $T_f$ are plotted as a function of $dG$ factor in Fig. 3a and b, respectively, for the pure RMgZn materials as well as $(Y_{1-x}Gd_x)$MgZn and $(Y_{1-x}Tb_x)$MgZn. Fig. 3a shows that the coupling between the local moments, as measured by $\theta$, scales with the $dG$ factor very well. This is consistent with the moments being coupled via the RKKY interaction. On the other hand, $T_f$

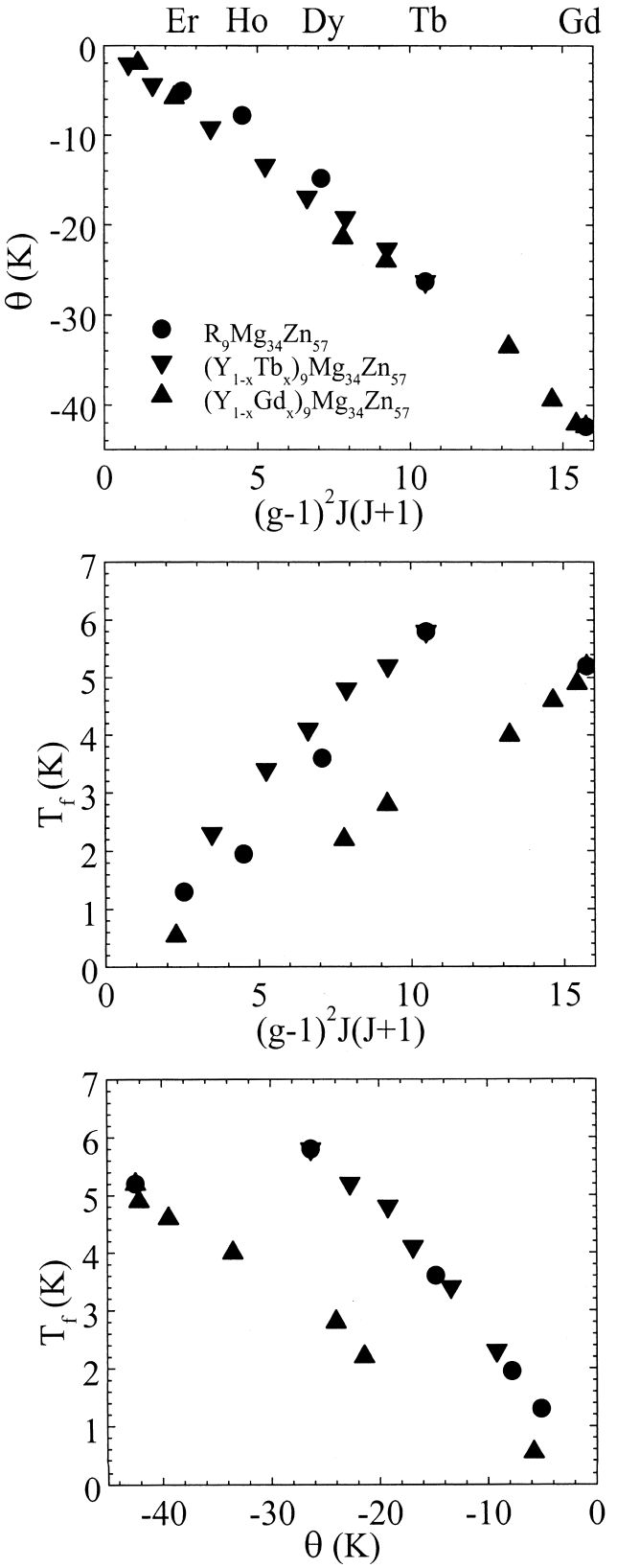


Fig. 3. (a) $\theta$ vs. $dG$ factor, (b) $T_f$ vs. $dG$ factor, (c) $T_f$ vs. $\theta$, for RMgZn compounds and pseudo-ternaries. Note: symbols on top horizontal axis indicate positions of pure RMgZn compounds.

(Fig. 3b) does not scale with the $dG$ factor nearly as well. There are essentially two manifolds in Fig. 3b, one for $Y_{1-x}Gd_xMgZn$, and another for all the remaining, local moment RMgZn compounds and alloys.

The origin of this difference is very likely associated with the crystalline electric field (CEF) splitting of the Hund's rule ground state multiplet. For Gd the total angular momentum, $L$, is zero and there is essentially no CEF splitting. As a result, in intermetallic compounds such as these the magnetic response of paramagnetic Gd is virtually isotropic, i.e. it acts like a Heisenberg moment. On the other hand, for Tb–Er, $L$ is finite and there can be significant CEF splitting. In many intermetallic systems this can be extreme [8–11]. Given that the number of unique rare earth crystallographic sites and their point symmetries are as of yet unknown for icosahedral RMgZn it is impossible to state that a given rare earth will be Ising-like, planar, etc. but it is safe to say that for RMgZn (R = Tb–Er) the moments will be non-Heisenberg.

The data in Figs. 3a and b can be plotted without the $dG$ factor as shown in Fig. 3c. In this case the experimentally determined $T_f$ is plotted against the experimentally determined $\theta$. The Heisenberg/non-Heisenberg separation is even clearer in this plot and no theoretical assumptions associated with the validity of $dG$ scaling were made.

The physical significance of these data is that there are at least two effects giving rise to the spin glass state. One is the distribution of R–R separations and the other is the distribution of easy axis (or plane) directions in the non-Heisenberg members. In essence then the freezing of the non-Heisenberg RMgZn compounds is governed by both of these effects whereas the freezing of the $Y_{1-x}Gd_xMgZn$, Heisenberg system arises solely from the distribution of Gd–Gd separations.

## 4. Mixed Heisenberg and non-Heisenberg systems

One obvious question that arises from the observed difference in freezing temperature between TbMgZn and GdMgZn is: what happens to the freezing temperature as we add non-Heisenberg moments to a Heisenberg system? A very rough analogy is to think of a floor covered with marbles and ask the question: how many non-spherical marbles have to be added to make the floor less slippery? Whereas this analogy does not fully capture the physics of the spin freezing phase transition it does give an idea of how the non-Heisenberg moments will initially lead to an increased freezing temperature.

Fig. 4 plots $\theta$ and $T_f$ of $(Tb_{1-x}Gd_x)MgZn$ as a function of $x$. Whereas $\theta$ scales roughly with $x$ and falls onto the data plotted in Fig. 3a, $T_f$ has an exceptionally non-linear and even non-monotonic $x$ dependence. Starting from pure TbMgZn, as $dG$ increases $T_f$ increases, as would be expected from the $dG$ scaling seen in Fig. 3b. So, initially the addition of Gd increases $T_f$ in response to the increase

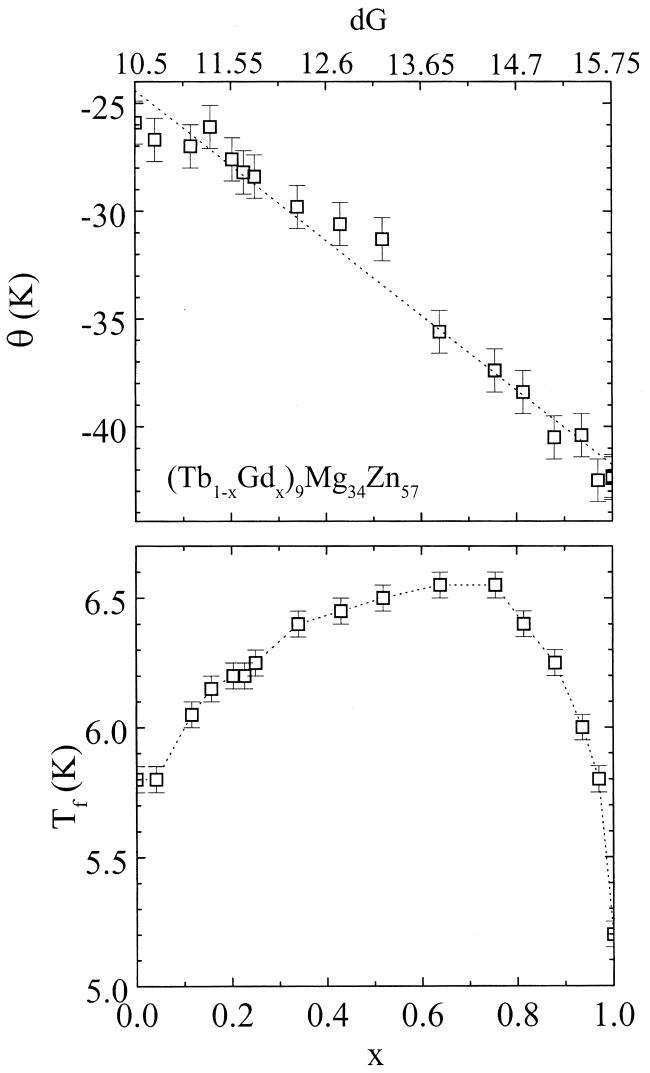


Fig. 4. (a) $\theta$ vs. $x$ and $dG$ factor, and (b) $T_f$ vs. $x$ and $dG$ factor for $(Tb_{1-x}Gd_x)MgZn$. The dotted lines are a guide to the eye.

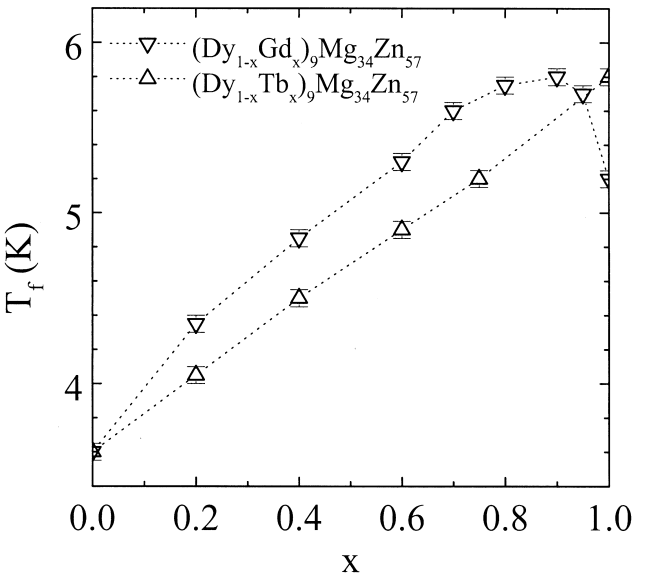


Fig. 5. $T_f$ vs. $x$ for $(Dy_{1-x}Gd_x)MgZn$ and $(Dy_{1-x}Tb_x)MgZn$. The dotted lines are a guide to the eye.

in the magnitude of $\theta$. This increase in $T_f$ holds for $x \lesssim 0.7$. For $x > 0.7$ there is a rapid drop of $T_f$ from a maximum value of ~6.6 K down to $T_f = 5.2$ K for pure GdMgZn. If we examine these data starting from the pure GdMgZn side we see that with the addition of the non-Heisenberg Tb (the non-spherical marbles in our analogy) there is a rapid increase in the freezing temperature. With as little as 30% Tb ($x = 0.7$) the freezing temperature is essentially on the manifold of freezing temperatures defined by the non-Heisenberg materials.

An objection that can be brought against the above analysis is that we have not taken the effects associated with the disordering of the rare earth site into account. We can address this experimentally by examining two other pseudo-ternary series: $(Dy_{1-x}Gd_x)MgZn$ and $(Dy_{1-x}Tb_x)MgZn$. Fig. 5 presents $T_f$ as a function of $x$ for both of these series. As can be seen whereas $T_f$ for $(Dy_{1-x}Tb_x)MgZn$ varies linearly with $x$, $T_f$ for $(Dy_{1-x}Gd_x)MgZn$ has a non-monotonic dependence on $x$ that is similar to that seen for $(Tb_{1-x}Gd_x)MgZn$ in Fig. 4b. The fact that there is a local maximum in $T_f$ seen in $(Dy_{1-x}Gd_x)MgZn$ but not in $(Dy_{1-x}Tb_x)MgZn$ strongly supports the assumption that this maximum represents a cross over from the non-Heisenberg to Heisenberg freezing as $x$ is increased for these compounds. It is worth noting that for both $(Tb_{1-x}Gd_x)MgZn$ and $(Dy_{1-x}Gd_x)MgZn$ the deviation from the non-Heisenberg $T_f(x)$ manifold occurs for $x \sim 0.7$.

## 5. Summary

Fig. 6 presents $T_f$ as a function of $\theta$ for all the ternary and pseudo-ternary single grains that we have examined so far (over 40 different compounds). The purely Heisenberg manifold of the $(Y_{1-x}Gd_x)MgZn$ is clearly visible, as is the higher $T_f$ non-Heisenberg manifold. Whereas $(Tb_{1-x}Gd_x)MgZn$ and $(Dy_{1-x}Gd_x)MgZn$ both have a local maximum in $T_f$ for $x \sim 0.7$–$0.8$ this does not appear at the same value of $\theta$ (or $dG$) due to the different values of the $dG$ factor for Tb and Dy. The fact that this maximum in $T_f$ appears to be related to the value of $x$ rather than the $dG$ factor or an energy scale such as $\theta$ implies that there may be a critical concentration (i.e. a percolation threshold) of non-Heisenberg moments needed to force the mixed system to fall on the non-Heisenberg $T_f(\theta)$ manifold. From these data it appears that roughly 30% of the Heisenberg moments need to be replaced with non-Heisenberg moments to force the compound to freeze like a non-Heisenberg spin glass.

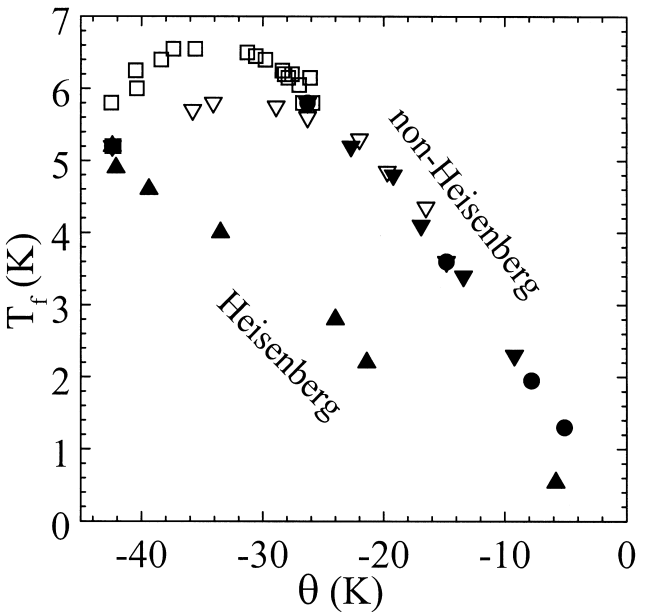


Fig. 6. $T_f$ vs. $\theta$ for all measured RMgZn compounds and pseudo-ternaries. The symbols are the same ones used and defined in earlier figures.

## Acknowledgements

We thank M.J. Kramer and A. Kracher for structural and compositional analysis and N. Anderson Jr. for help with sample preparation. P.C.C. has been supported in part by the C.E.A., Grenoble during the preparation of this work. Ames Laboratory is operated for the U.S. Department of Energy by Iowa State University under Contract No. W-7405-Eng-82. This work was supported by the Director of Energy Research, Office of Basic Energy Sciences.

## References

[1] I.R. Fisher, Z. Islam, A.F. Panchula, K.O. Cheon, M.J. Kramer, P.C. Canfield, A.I. Goldman, Philos. Mag. B 77 (1998) 1601.
[2] A. Langsdorf, F. Ritter, W. Assmus, Philos. Mag. Lett. 75 (1997) 381.
[3] P.C. Canfield, Z. Fisk, Philos. Mag. B 65 (1992) 1117.
[4] I.R. Fisher, M.J. Kramer, Z. Islam, T.A. Wiener, A. Kracher, A.R. Ross, T.A. Lograsso, A.I. Goldman, P.C. Canfield, Mater. Sci. Engineer. A (in press).
[5] I.R. Fisher, K.O. Cheon, A.F. Panchula, P.C. Canfield, M. Chernikov, H.R. Ott, K. Dennis, Phys. Rev. B 59 (1999) 308.
[6] I.R. Fisher, M.J. Kramer, T. Wiener, Z. Islam, A.R. Ross, T.A. Lograsso, A. Kracher, A.I. Goldman, P.C. Canfield, Philos. Mag. B 79 (1999) 1673.
[7] I.R. Fisher, M.J. Kramer, Z. Islam, A.R. Ross, A. Kracher, T. Wiener, M.J. Sailer, A.I. Goldman, P.C. Canfield, Philos. Mag. B 79 (1999) 425.
[8] P.C. Canfield, P. Gammel, D. Bishop, Physics Today 51 (No. 10) (1998) 40.
[9] S.L. Bud'ko, P.C. Canfield, C.H. Mielke, A.H. Lacerda, Phys. Rev. B 57 (1998) 13624.
[10] K.D. Myers, S.L. Bud'ko, I.R. Fisher, Z. Islam, H. Kleinke, A.H. Lacerda, P.C. Canfield, J. Magn. Magn. Mater. 205 (1999) 27.
[11] S.L. Bud'ko, Z. Islam, T.A. Wiener, I.R. Fisher, A.H. Lacerda, P.C. Canfield, J. Magn. Magn. Mater. 205 (1999) 53.